RSC Advances

PAPER

View Article Online
View Journal | View Issue

Cite this: *RSC Adv.*, 2016, **6**, 17256

Modification of nanostructured ZnO surfaces with curcumin: fluorescence-based sensing for arsenic and improving arsenic removal by ZnO

Rasha N. Moussawi and Digambara Patra*

Applying a simple aqueous phase chemistry method, nanostructured zinc oxide surfaces have been modified with curcumin, here referred to as Zn(cur)O. The morphology of these Zn(cur)O nanostructured materials is a grain-like wurtzite hexagonal crystal structure with good crystalline quality. Doping of curcumin fills the defects of ZnO that are visible luminescence centers and prolongs electron–hole recombination, resulting, respectively, in quenching of visible luminescence and an enhancement in the exciton emission of ZnO. The photoluminescence of ZnO is insensitive to arsenic concentration in water, but the photoluminescence of a Zn(cur)O colloidal solution at an excitation wavelength of 425 nm can sensitively sense arsenic in the concentration range 100 to 3000 ppb. At the same time Zn(cur)O can significantly improve the efficient removal of arsenic contamination from water below the maximum contaminant level (MCL) within 30 minutes and almost to zero in 3 h without oxidation and/or pH adjustment. The adsorption kinetics during arsenic removal by Zn(cur)O obeys a pseudo-second order model with exceptional adsorption rates compared to ZnO, reflecting the high affinity of Zn(cur)O nanomaterials to arsenic due to improvement in adsorption.

Received 30th September 2015
Accepted 4th February 2016

DOI: 10.1039/c5ra20221c

www.rsc.org/advances

1. Introduction

The design of functional nanomaterials has fuelled the advance of nanomaterials and nanotechnology through the production of special materials with novel properties for potential applications in chemical, biological, and technological domains. Incorporating functionalities of organic systems on the surface of metal oxide nanoparticles will yield hybrid materials with novel properties and functions.[1,2] Zinc oxide has presented itself as a special material with great potential and thus has attracted research to study this semiconductor in the form of powders, single crystals, thin films, or nanostructures. ZnO has a wide band gap (~3.37 eV at room temperature[3]) and its high exciton-binding energy (60 meV)[3] allows efficient excitonic emission even at room temperature.[4] Although a small amount of ZnO dissolves and releases zinc ion into water, ZnO is biocompatible rendering it suitable for biomedical and environmental applications such as, transparent conducting electrodes in solar cells,[5] photocatalysts for degradation of organic pollutants in wastewaters,[6] UV lasers,[7] and chemical and biological sensors.[8]

Arsenic contamination in natural water renders the lives of millions of people around the world at risk. Exposure to arsenic over extended periods of time leads to serious health problems, such as cancers of liver, lung, kidney, bladder, and skin,[9,10] cardio vascular system problem,[11] and affects the mental development of children.[12] Arsenic in natural water can be the result of leaching from arsenic containing source rocks and sediments. Its presence is generally associated to geochemical environments such as basin-fill deposits of alluvial lacustrine origin, volcanic deposits, inputs from geothermal sources, mining wastes and land fills.[13,14] In 2001, the US Environmental Protection Agency (EPA) lowered the maximum contaminant level (MCL) for arsenic in drinking water from 50 to 10 μg L^{-1} (0.01 ppm)[15] which rendered the drinking sources all over the world unacceptable. The arsenic contamination of the groundwater has been a serious problem in many countries. Therefore, research on arsenic detection and removal from drinking water using low-cost and simple methods has greatly increased. The conventional methods[15] for arsenic treatment include coagulation and flocculation, precipitation, adsorption, ion exchange, and membrane filtration. Alternative unconventional methods like ozone oxidation, bioremediation and electro-chemical treatments are also used in the removal of arsenic. Among the various arsenic removal techniques, adsorption seems to be the simplest, cost-effective, and safer to handle process than precipitation, ion exchange, and membrane filtration.

Arsenic exists in water as two major inorganic arsenic species, namely As(III) (arsenite, AsO_3^{3-}) and As(V) (arsenate, AsO_4^{3-}). The existence and ratio of these two forms of arsenic is dependent greatly on pH and the redox conditions of the environment in which they are present. Arsenates are stable under aerobic or oxidizing conditions, while arsenites are stable under

Department of Chemistry, American University of Beirut, Beirut, Lebanon. E-mail: dp03@aub.edu.lb; Fax: +961 1 365 217; Tel: +961 1 350 000 ext. 3985

anaerobic or mildly reducing conditions.[15] Arsenite species exists in solution as H_3AsO_3 (arsenous acid) and $H_2AsO_3^-$ (dihydrogen arsenite) with pK_a values of 9.2 and 12.7 respectively.[16] Arsenate species is present as $H_2AsO_4^-$ (dihydrogen arsenate) and $HAsO_4^{2-}$(arsenate hydrogen ion) and the pK_a values for arsenic acid (H_3AsO_4) are pK_{a1} = 2.3, pK_{a2} = 6.8, and pK_{a3} = 11.6.[16] Of these two redox states of As, arsenite As(III) is the more toxic form than arsenate. Also, arsenate is easier to remove from water than arsenite, as it is an ionic species in the pH range typically found in the aquatic environment.[17] Arsenite, on the other hand, exists in nonionic form H_3AsO_3 in natural water with pH value ranging from weakly acidic to weakly alkaline, which renders the adsorption performance of various adsorbents on As(III) poor.[18–20] It would require additional oxidizers to oxidize arsenite to arsenate if pH is less than 10.[17] Thus, oxidizing As(III) to As(V) and/or pH adjustment becomes necessary for its effective removal from water before coagulation–precipitation or adsorption processes.[21–23] As this would add to the complexity and cost of the treatment process, adsorbents able to effectively remove As(III) without the oxidation/pH adjustment is being developed.

ZnO acts as a good adsorbent, but so far it has its own limitations. Doping with organic system may influence adsorption and luminescence properties of ZnO. The sensitization of ZnO towards visible light means the band gap has to be narrowed or split into several sub-gaps. This has been done through various methods such as surface modification by incorporation of organic materials,[24] fullerenes[25] and polymers.[26–28] However, research work on dye doped zinc oxides and their respective optical and catalytic properties remains narrowed. Curcumin (see Scheme 1) accounts as the major component in the curcuminoid complexes and well known for its pharmaceutical applications and medicinal potential in therapy of many diseases such as, cancer, cardiovascular disease, and rheumatoid arthritis.[29–31] Reports on curcumin as sensitizer are scarce. Curcumin-derived dye can be used as a sensitizer in dye sensitized solar cells with photocurrent density of 1.66 mA cm^2.[32] Curcumin has very exciting photophysical and fluorescence properties.[33] Curcumin, as fluorescence probe for developing new sensing scheme, is getting widely realised.[34–36] It can act as a reducing agent to prepare metal nanoparticles[37] and nanorods[38] and make metal complex with various metal ions.[39–41] It also forms a Zn–curcumin complex by reacting with zinc salt.[42] Curcumin has also been used to prepare ZnO–curcumin composites.[43–45] However, there is no literature work where curcumin is doped on ZnO surfaces. In this work we attempted to prepare a new curcumin doped ZnO nanomaterials, which is termed here as Zn(cur)O, and apply it for developing new fluorescence sensing scheme for arsenic as depicted in Scheme 2 and at the same time quick removal of arsenic from water without the oxidation and/or pH treatment.

2. Materials and methods

2.1 Materials

Zinc nitrate hexahydrate ($Zn(NO_3)_2 \cdot 6H_2O$) (98% extra pure) was obtained from Acros Organics. Curcumin was received from Sigma and acetone (HPLC grade) was used from Aldrich. Potassium hydroxide was sourced from AnalaR. A primary stock element reference solution of arsenic (As(III), 1000 ppm, matrix: 0.5 M HNO_3) was supplied by Romil LTD and stored in the dark in a refrigerator. All the solutions were prepared with deionized water unless otherwise mentioned.

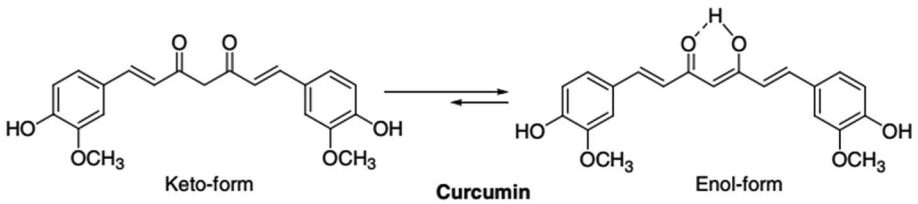

Scheme 1 Structure of curcumin.

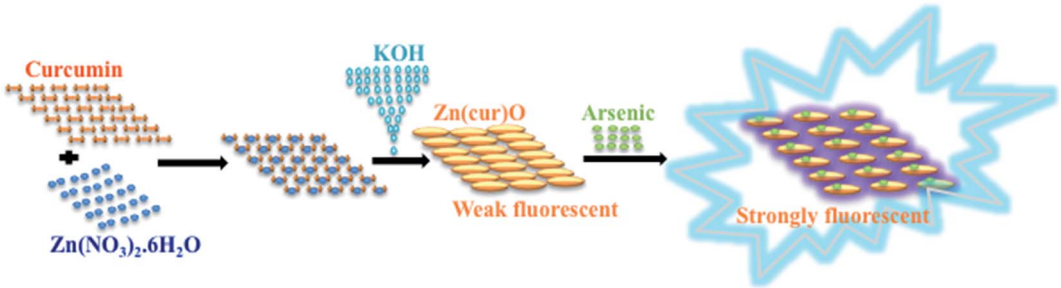

Scheme 2 Schematic illustration of synthesis of Zn(cur)O followed by fluorescence enhancement of Zn(cur)O upon binding with arsenic in water.

2.2 Synthesis

Zn(cur)O was prepared by taking 0.5 (±0.1) mg, 1.0 mg (±0.1), or 2.0 (±0.1) mg of curcumin in 50 mL of double distilled water (close to neutral pH) at 80–90 °C. The relatively high temperature was useful for ZnO synthesis. When curcumin was solubilized completely, 50 mL of 0.1 M $Zn(NO_3)_2$ solution prepared in double distilled water was added to it. The yellowish solution was refluxed for 1 hour at 85–90 °C. After that, the solution was cooled down and 5 mL of 0.2 M KOH was added slowly at 4 °C. An orange yellow gel-like suspension was observed. The solution was centrifuged at 5000 rpm and the precipitate was washed with water till no more yellow color was observed in the supernatant. Acetone washes were necessary to remove any unanchored curcumin after which the final wash was with water. The precipitate Zn(cur)O was vacuum dried at room temperature. A control ZnO was synthesized by taking 50 mL of 0.1 M $Zn(NO_3)_2$ solution prepared in double distilled water and then adding 5 mL of 0.2 M KOH slowly in an ice bath at 4 °C. The white suspension was centrifuged at 5000 rpm, washed with water and vacuum dried just like Zn(cur)O.

2.3 Characterization

Scanning electron microscopy (SEM) analysis was carried out using Tescan, Vega 3 LMU with Oxford EDX detector (Inca XmaW20) SEM. The sample was deposited on a carbon film for SEM analysis. The fluorescence image was recorded using a high sensitive STED confocal set up consisted of confocal microscope (Leica TCS SP5 STED, Leica Microsystem), APD detector and an argon laser with 430 nm excitation wavelength. Zn(cur)O was excited by a wavelength of 430 nm and typical emission wavelengths were 490–600 nm. The X-ray diffraction (XRD) data were recorded using a Bruker d8 discover X-ray diffractometer equipped with Cu-Kα radiation ($\lambda = 1.5405$ Å). The monochromator used was Johansson type. The step size was 0.02 s and the scan rate was 20 s per step.

2.4 Spectroscopic analysis

The chemical structures of Zn(cur)O and, ZnO were characterized by FTIR spectroscopy. A Thermo Nicolet 4700 Fourier Transform Infrared Spectrometer equipped with a Class 1 laser was used for this purpose. The KBr pellet technique was applied to perform the transmission experiments in the range between 4000 and 400 cm^{-1}. The absorption spectra were recorded at room temperature using a JASCO V-570 UV-VIS-NIR Spectrophotometer. Similarly, UV-visible diffuse reflectance spectra were measured using the same spectrophotometer in the range 200 to 800 nm. The steady-state photoluminescence/fluorescence spectra were recorded at room temperature using Jobin-Yvon-Horiba Fluorolog III fluorometer and the FluorEssence program where the excitation and emission slits width were 5 nm. The source of excitation was a 100 W xenon lamp, and the used detector was R-928 operating at a voltage of 950 V.

2.5 Adsorption study

For As(III) removal experiment, the same general procedure was followed for different concentrations of arsenic using samples of Zn(cur)O that differ by their curcumin content. Using 1 ppm As(III) stock solution, 100 ppb and 903 ppb arsenic concentrations were prepared in a final volume of 12 mL. The pH of the solution was about 6. After adding the Zn(cur)O, the arsenic solution was placed on the vortex (speed was no more than 1200 rpm) and left shaking to disperse Zn(cur)O particles and ensure its good contact with the arsenic contamination. Based on the linear dynamic range indicated in the manual for arsenic measurements of the instrument used, we set a low and a high standard concentration of 7 ppb and 55 ppb respectively. With proper dilutions, the samples were set to a final maximum arsenic concentration of 50 ppb. Portions of 1 mL were withdrawn at different time intervals, and dumped directly into a 1 mL deionized water to obtain a final concentration of 50 ppb as a maximum. For the high arsenic concentration (903 ppb), proper dilution was also done. After dilution, the samples were filtered using a general use filter paper. The experiments were done in duplicate or triplicate and each measurement was repeated twice. For each set of measurements done together (7–8 samples), a series of 6 or 8 standards were freshly prepared. Measurements of arsenic concentration were analyzed by SOLAAR atomic absorption spectrophotometer (Thermo Labsystems) with ASX-510 autosampler, G95 graphite furnace, FS95 furnace autosampler, PLATON Hg sampling, MILESTONE Ethos Plus microwave labstation, and SOLAAR data acquisition and analysis computer software. The percentage adsorption of arsenic on adsorbate from aqueous solution was calculated as follows:

$$\text{Adsorption (\%)} = [(C_{\text{int}} - C_{\text{fin}})/C_{\text{int}}] \times 100$$

where C_{int} and C_{fin} are the initial and final arsenic concentrations in the solution, respectively.

3. Results and discussion

Briefly, Zn(cur)O nanoparticles were prepared through wet chemistry in which curcumin and zinc nitrate were mixed at 85–90 °C for 2 hours and the yellow colored solution was cooled to 0 °C in an ice bath, subsequently potassium hydroxide solution was added slowly. The yellowish precipitate obtained, Zn(cur)O, was centrifuged and washed. It should be noted that curcumin degrades in alkaline medium,[46] but addition of potassium hydroxide to curcumin and zinc nitrate did not show any appreciable degradation or change in colour of curcumin. Zn($x$cur)O (where $x = 0.5$, 1.0, or 2.0) particles were synthesized respectively by using 0.5 mg, 1.0 mg, or 2.0 mg of curcumin. Washing of Zn(cur)O with acetone didn't alter its yellowish colour and no curcumin was detected in the wash solution. ZnO control was prepared without using curcumin.

The SEM images of the as synthesized ZnO and Zn(cur)O nanoparticles are presented in Fig. 1. The particles were of sizes ranging from 200–600 nm width and 600–2000 nm length. There were also particles of smaller sizes. The particles looked

similar to grain or half grain. Zn(cur)O particles were found to be not different in their appearance and morphology compared to ZnO. Closer SEM images of these grain shaped Zn(cur)O were recorded in 200 nm resolution as shown in Fig. 2a, which shows that these grain appearing particles were assembled of nano-sized particles. It should be noted that changing the concentration of curcumin (0.5 mg, 1.0 mg, or 2.0 mg) during preparation of Zn(cur)O did not have any foremost impact on the morphology of these particles, although Zn(cur)O prepared using 2 mg curcumin were found to have more number of smaller or half-broken particles (Fig. 2b). The morphology of these particles was also clearly visible in fluorescence STED microscope (Fig. 3a). The fluorescence coming out from the whole region indicates curcumin is present all over the particle in Zn(cur)O. Amount of curcumin both on the surface and the inside of ZnO was estimated by thermogravimetric analysis. In between 100 and 700 °C, the weight loss for naked ZnO was ~4% and that of Zn(cur)O was ~24%. Based on these data the amount of curcumin in Zn(cur)O was estimated to be ~20%.

The XRD pattern of ZnO and Zn(cur)O is shown in Fig. 3b. All the Zn–O hexagonal phase diffraction peaks were found at 2θ of 31.80° (*h k l*, 100), 34.51° (*h k l*, 002), 36.26° (*h k l*, 101), 47.49° (*h k l*, 102), 56.61° (*h k l*, 110), 62.99° (*h k l*, 103), 66.55° (*h k l*, 200), 67.84° (*h k l*, 112), 69.19° (*h k l*, 201) and 77.53° (*h k l*, 202). These observed peaks are in good agreement with those for hexagonal ZnO with wurtzite structure as reported earlier.[47] The additional peaks found at 37.03°, 37.80°, 43.23° and, 64.35° were attributed to curcumin. The sharp diffraction peaks apparent in the figures indicate good crystallinity of the ZnO nanoparticles. No characteristic peaks of any other phase of ZnO or of any impurity were observed which indicates the relatively good purity of the compounds. The pattern of pure curcumin showed sharp characteristic peaks[48] at 2θ of 20–30°. However, the characteristic peaks of curcumin were not observed when coated on ZnO in the XRD patterns of Zn(0.5cur)O and Zn(1.0cur)O, and only three peaks at 26.0, 26.8, and 29.45 for Zn(2.0cur)O were attributed to curcumin in this range. The Scherrer equation[49] relates average crystallite size of the sample with the line broadening at full width at half maximum (FWHM) and thus the average crystallite sizes of samples were determined using the Scherrer equation:

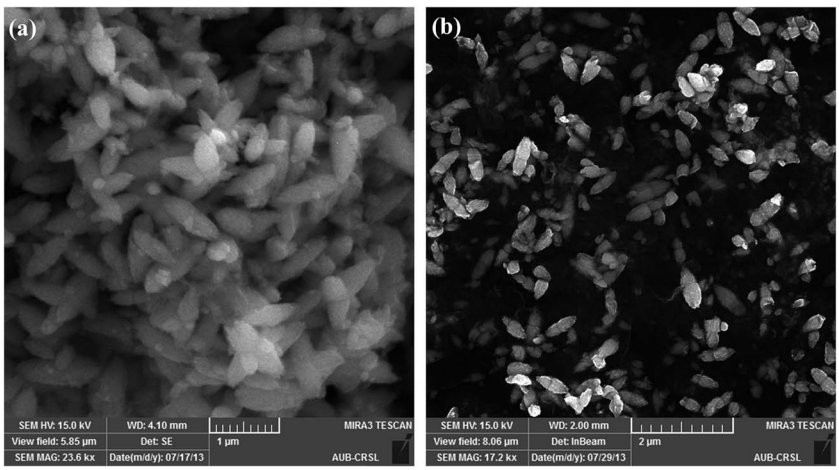

Fig. 1 SEM images of (a) ZnO and (b) curcumin doped ZnO which is termed as Zn(cur)O.

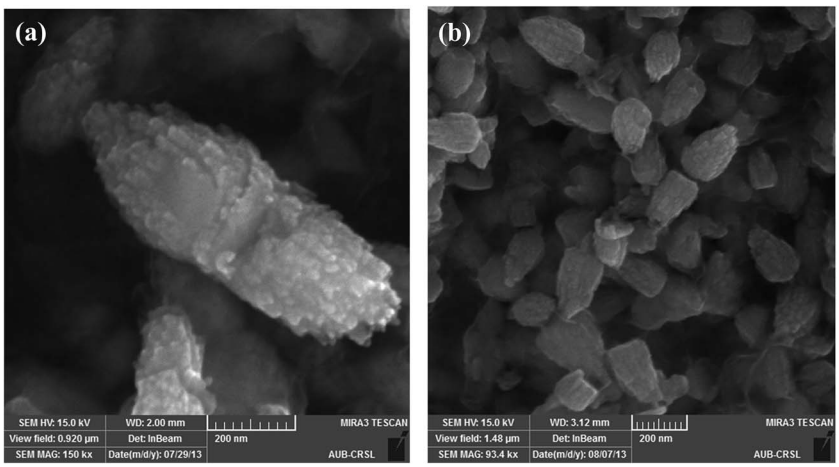

Fig. 2 SEM images of (a) Zn(0.5cur)O where [cur] = 0.5 mg and (b) Zn(2.0cur)O where [cur] = 2.0 mg.

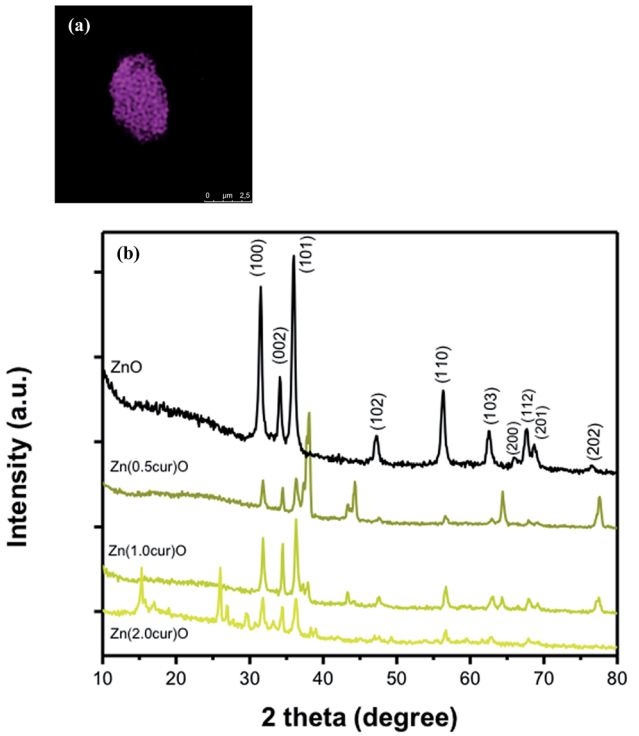

Fig. 3 (a) STED fluorescence image of Zn(cur)O; (b) X-ray diffraction patterns of ZnO, Zn(0.5cur)O, Zn(1.0cur)O and Zn(2.0cur)O nanoparticles.

$$D_{\mathrm{XRD}} = 0.9\lambda\beta/\cos\theta$$

where D_{XRD} is the average crystallite sizes (nm), λ the X-ray wavelength ($\lambda = 1.5406$ Å), β the full-width at FWHM of the highest intensity peak in radians, and θ the half of diffraction peak angle. The peak of the [100] plane (one of the strong peaks) was monitored to evaluate relative crystallite size with respect to curcumin concentration used during synthesis of Zn(cur)O. Crystallite sizes of 24.63 nm, 20.18 nm, 26.06 nm, and 20.04 nm were obtained for ZnO, Zn(0.5cur)O, Zn(1.0cur)O, and Zn(2.0cur)O respectively. This change is marginal without giving any specific relationship between crystalline structures and the amount of curcumin used in Zn(cur)O.

FTIR spectroscopy was done to inspect the interaction of curcumin with ZnO through the fingerprint vibrations of both curcumin and ZnO and of Zn(cur)O as shown in Fig. 4. Bare ZnO showed strong and broad absorption peak around 442 cm^{-1}, which is the characteristic of Zn–O bond.[50] No bands appeared around 3500 cm^{-1} nor at 1600 cm^{-1} which are usually attributed to O–H stretching vibration peak of the hydroxyl functional group and to the bending vibration of the surface H–OH, which means that no hydroxyl groups adsorption on the surface of ZnO took place and what we had was ZnO rather than $Zn(OH)_2$. The peak at 442 cm^{-1} in ZnO shifted to 484 cm^{-1} in Zn(cur)O and was less pronounced suggesting the presence of an altered Zn–O bond due to its interaction with curcumin.

The frequency region of both phenolic ν(OH) vibrations of the curcumin was computed to be at 3595 cm^{-1}, but was shifted to lower frequency at 3510 cm^{-1} due to intramolecular and intermolecular H-bonding in curcumin.[51] In Zn(cur)O the location of the band shifted to 3430 cm^{-1} indicating interaction of these phenolic hydroxyls with ZnO. Curcumin molecule has one of the most prominent functional group—the β-diketone group—at the center, which has high driving force to form chelation with metal ions.[40,42] The β diketo system in curcumin was found to form charge transfer complexes with TiO_2 nanoparticles.[52] Khalil *et al.* have suggested a four coordination zinc–curcumin complex through β diketo system based on mass spectral data.[42] This could be due to the co-existence of keto and enol groups in curcumin molecules. In this respect, it is not surprising to have an interaction—be it weak or strong—of this β-diketone moiety with Zn atom at the bulk surface of ZnO. In fact, the curcumin spectra did not show any peak in the carbonyl region (1800–1650 cm^{-1}) as reported earlier, neither in the solid state nor in solutions, indicating that curcumin exists mainly in the enol form. However, two peaks were obtained in this region at ~1650 cm^{-1} and at 1756 cm^{-1} for the ZnO–curcumin compound, where the 1650 cm^{-1} peak could be due to ν(C=O) of curcumin. The other peak at 1756 cm^{-1} could be related to the carbonyl's asymmetric mode of vibration in its diketo solid form (the symmetric mode is unseen usually because its intensity is too low). Theoretical calculations show that the enolic ν(OH) mode is at 2979 cm^{-1}.[51] Experimentally, this band usually appears weak and broad as it did in this case. The absence of a clearly defined ν(OH) band has been previously discussed by Tayyari *et al.*[53] stating that "the intensity and broadness of the enol band is dependent on the strength of the intramolecular hydrogen bond where it would decrease in intensity and increase in broadness as the strength of the hydrogen bond increases". Also in their work on dibenzoylmethane, a β-diketone system, similar to curcumin, they have suggested that the π-systems, such as the phenyl groups increase the H-bond strength through conjugation with the enol ring. The hydroxyl and methoxy groups on the phenyl rings of curcumin are electron donating systems expected to even cause stronger hydrogen bond effect. So any weakening of these groups' electronegativity (phenyl ring and/or the existing methoxy and hydroxy groups on it) by forming bonds or conjugating with other moieties would cause the hydrogen bond strength to decrease thus allowing the enol peak to appear more clearly. In our Raman spectroscopic measurement the Raman band at 1601 cm^{-1} was obtained for curcumin due to aromatic vibration $\nu_{\mathrm{C=C\ ring}}$ and this band shifted to 1593 cm^{-1} in Zn(cur)O. Therefore, one of the possibilities does not rule out involvement of the ZnO with the hydroxyl or methoxy groups on the phenyl ring.

However, the prominent enol peak could also be due to chelation of curcumin with metal ions as suggested earlier for zinc–curcumin complex.[42] In our FT-IR measurement, the peak in curcumin at ~1630 cm^{-1} has a predominantly mixed ν(C=C) and ν(C=O) character. The most prominent band in the curcumin spectrum was found at 1510 cm^{-1} attributed to highly mixed vibrations of ν(C=O), δ(CC=O), and δ(CCC).[51] The IR bands in frequency region 1430–1460 cm^{-1} are due to deformation vibrations of the two methyl groups. Most bands in

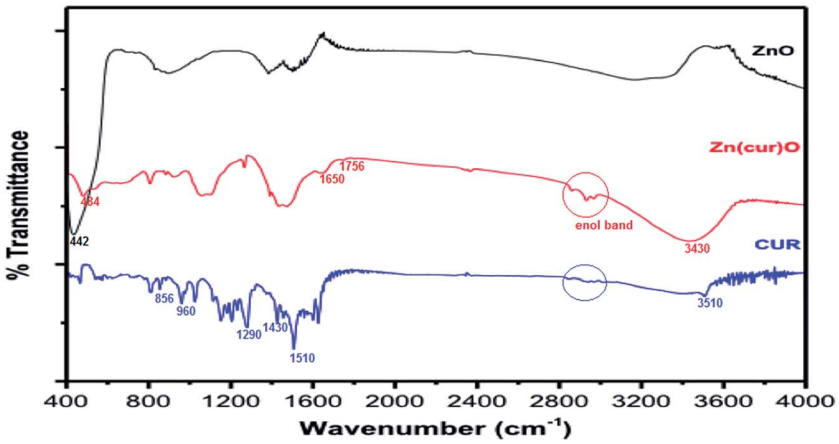

Fig. 4 FTIR spectra of as-synthesized ZnO, curcumin, and Zn(1.0cur)O nanostructures at room temperature.

frequency region 1450–1300 cm^{-1} are highly mixed. Similarly, the Raman shift at 1626 cm^{-1} was found for curcumin, which is due to $\nu_{C=C}$ and $\nu_{C=O}$ of curcumin and similar to reported experimental value and close to computed values 1630 cm^{-1} and 1615 cm^{-1} respectively.[51] In Zn(cur)O this band shifted up field to 1630 cm^{-1} indicative of a relatively strong coordination of the carbonyl moiety.[54] The Raman band at 1314 cm^{-1} is due to $\delta_{PhCCHOHenol}$. The Raman peak at 1304 cm^{-1} for $\delta_{COHenol}$ was not found in curcumin, but was observed for Zn(cur)O. The band at 1248 cm^{-1} due to $\delta_{COHenol}$ of curcumin also shifted to around 1224 cm^{-1} in Zn(cur)O indicating presence of CO type bond associating with zinc. The carbonyl and hydroxyl groups of curcumin can form chelate with zinc. This could also be supported by the disappearance and shifting of the IR bands at 960 and 855 cm^{-1} in Zn(cur)O (see Fig. 4), which are attributed to ν(C–O) vibrations. Present spectroscopic analysis supports that curcumin chelates with zinc through enol form but at the same time a weak link between hydroxyl or methoxy groups on the phenyl ring and ZnO exists.

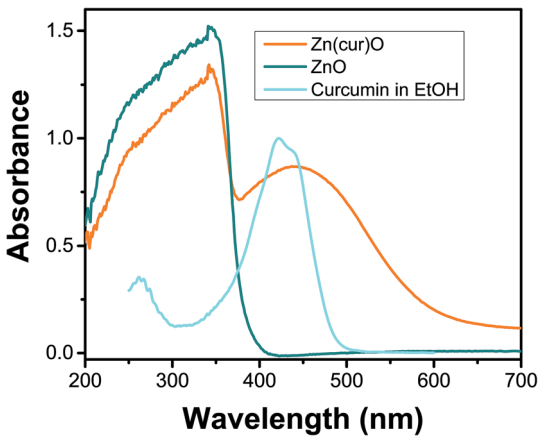

Fig. 5 UV-visible diffuse reflectance spectra of as-synthesized ZnO, and Zn(1.0cur)O nanostructures at room temperature. UV-visible absorption spectrum of curcumin in ethanol is shown for comparison.

UV-Vis diffused reflectance spectra of the Zn(cur)O and ZnO are depicted in Fig. 5. All of them show a similar broad and strong absorption spectrum with an onset at 400 nm and a maximum at about 343 nm, which is characteristic of ZnO wide-band semiconductor. For Zn(cur)O, another strong absorption maximum was found at around 445 nm with an absorption onset at ~570 nm for Zn(cur)O confirming the presence of curcumin. As seen for curcumin in ethanol, the position of the curcumin peak in Zn(cur)O is red shifted compared to curcumin in solution. This shift in absorption spectra could be due to the interaction of curcumin with zinc ion that decreases the band gap between π–π^* electronic transition of curcumin.

The photoluminescence (PL)/fluorescence of Zn(cur)O and ZnO were measured at two excitation wavelengths: 320 nm (for ZnO excitation), and 425 nm (for curcumin excitation) in water and compared in Fig. 6. At 320 nm excitation wavelength (see Fig. 6a), ZnO showed two emission bands, one in the UV range at around 358 nm, which is associated with exciton emission, another in the visible range at around 560 nm, which originates from electron–hole (e–h) recombination at the deep level caused by oxygen vacancy or zinc interstitial defects.[55] This result – the observation of a visible PL in water – by itself is unconventional and interesting given the fact that even small amounts of water would kill ZnO PL – namely visible fluorescence – as hydroxyl groups coordinate on the surface of ZnO nanoparticles. Curcumin usually shows fluorescence in this region (around 530 nm),[33] however its contribution in Zn(cur)O was minimum or negligible. The visible photoluminescence in Zn(cur)O reduced by ~10 folds compared to naked ZnO. Similar quenching of visible emission has been observed and reported for capped ZnO compared with the uncapped ZnO.[55] Interestingly, in comparison to ZnO, the UV emission of Zn(cur)O at 358 nm increased by ~4 fold. This trend has been related earlier to increased crystallinity and decreased surface defects.[56] Some polymer and/or organic ligands are thought to fill up (passivate) the defects on ZnO surface, which act as visible luminescence centers, resulting in quenching the ZnO visible emission and

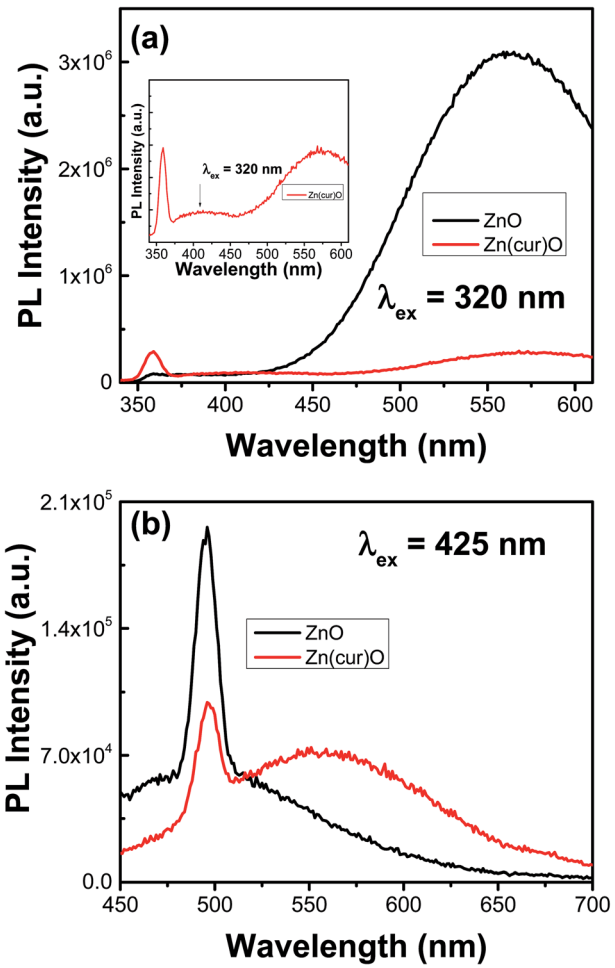

Fig. 6 Photoluminescence/fluorescence spectra of as-synthesized ZnO, and Zn(1.0cur)O nanostructures in water.

improving the UV emission.[55] This is what we think curcumin is doing. It is important to point out that the visible emission from ZnO cannot be fully explained by a single type of defect.[57] The visible emission band of Zn(cur)O was found to be 10 nm red shifted compared to that of ZnO. Zn(cur)O gave an additional band at around 405 nm (see inset of Fig. 6a) that was absent in ZnO. The emission line at 405 nm could be also related to defect emission caused by curcumin because we don't see any such peak in ZnO. At excitation wavelength of 425 nm (Fig. 6b), ZnO is not expected to have a good photoluminescence behavior due to poor light absorption in contrast to Zn(cur)O, which has a strong light absorption at this wavelength due to curcumin. Thus, the contribution of fluorescence of Zn(cur)O relative to ZnO is substantial at this excitation wavelength and the emission is largely due to curcumin rather than ZnO, as seen for curcumin alone in water at ~530 nm.[33] The peak at 495 nm in both the cases was due to scattering.

Subsequently, we tested photoluminescence behavior of ZnO and Zn(cur)O for the determination of arsenic. The sensing of arsenic was done for two concentration ranges: from 0 to 1000 ppb (1 ppm) and from 1 ppm to 10 ppm; thus, stock solutions of respectively 3000 ppb and 30 ppm of arsenic in water were used for this purpose. ZnO didn't show any systematic photoluminescence alteration in both the ranges of arsenic concentrations used at excitation wavelengths 280 nm and 425 nm (not shown), which limit use of ZnO to sense arsenic. However, Zn(cur)O showed an enhancement in fluorescence intensity with increasing arsenic concentration from 1 to 10 ppm as presented in Fig. 7. The binding mode of arsenic with ZnO surfaces has been experimentally established earlier,[58] it has been found that surface absorption is the main cause of As(III) binding on ZnO surface. In the present case surface adsorption of As(III) on Zn–O surfaces facilitate As(III) to come near to curcumin present in Zn(cur)O surfaces and interact on the phenyl rings and/or the hydroxyls groups as proposed subsequently. The enhancement of fluorescence could be linked with absorption of arsenic with Zn(cur)O surfaces. After removing arsenic from the Zn(cur)O surfaces, the same materials can be reused.

To comprehend effect of curcumin concentration in Zn(cur)O, a comparison was made for response for Zn(1.0cur)O and Zn(2.0cur)O as depicted in Fig. 8a in the concentration rage 0 to 1000 ppb and both of them showed good linear change in fluorescence signal. The higher sensitivity for Zn(2.0cur)O is due to higher fluorescence of Zn(2.0cur)O compared to Zn(1.0cur)O because of more curcumin content in Zn(2.0cur)O. Further, Zn(2.0cur)O was chosen because of higher sensitivity and the response was extended up to 10 000 ppb (10 ppm) using Zn(2.0cur)O as fluorescence probe for sensing application. As shown in Fig. 8b the fluorescence response showed an exponential increase and at higher concentration it started saturating. From Fig. 8b it can be estimated that the linear changes for sensing application is valid till around 3000 ppb of arsenic, where the present method could be applicable to determine arsenic in water samples. The detection limit estimated was 100 ppb.

The potential application of the curcumin doped ZnO system for arsenic removal was established in comparison with naked ZnO. The same general procedure was followed for different concentrations of arsenic, mainly 100 and 903 ppb, using samples of Zn(cur)O that differ by their curcumin content. Briefly, a stock of 200 ppm Zn(cur)O (and ZnO) solution was

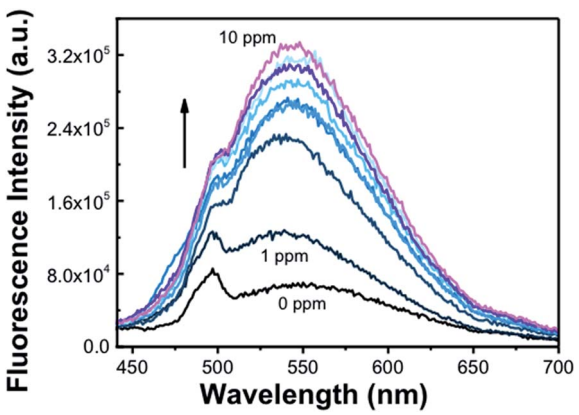

Fig. 7 Fluorescence sensing of arsenic in the concentration range 1 to 10 ppm using Zn(1.0cur)O.

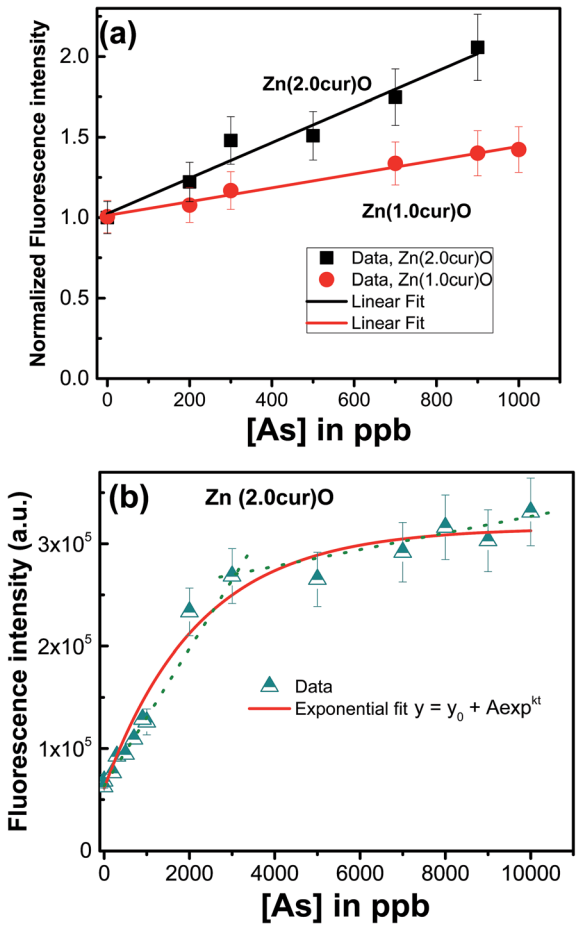

Fig. 8 (a) Fluorescence intensity response of Zn(1.0cur)O and Zn(2.0cur)O in the arsenic concentration range 0 to 100 ppm. (b) Fluorescence intensity response of Zn(2.0cur)O in the arsenic concentration range 1 to 10 000 ppb. The excitation wavelength used was 425 nm and emission wavelength was 550 nm.

prepared by mixing 1 mg of the compound in 5 mL deionized water. A secondary stock of 1 ppm of arsenic was prepared from a primary stock, As_2O_3 As(III) oxide, 1000 ppm. The stock solution was diluted to two initial As(III) concentrations, 903 μg L^{-1} and 100 μg L^{-1} (as 903.2 μg L^{-1} falls in the high range of arsenic specie concentration found in natural water around the world, and 97.8 μg L^{-1} is in the middle to low range[59]). For removal and adsorption study, arsenic was estimated by atomic absorption spectrophotometer. When the initial As(III) concentration was 100 ppb (see Fig. 9a), it was found that in just 30 minutes ~85, ~93.6, and ~90% of As(III) in the water sample could be removed with Zn(0.5cur)O, Zn(1.0cur)O, and Zn(2.0cur)O respectively, leaving arsenic concentrations below maximum contaminant level (MCL) [7.865, 3.0845, and 4.679 respectively]. After 3 hours, the equilibrium As(III) concentration in the water sample was less than 5 ppb after the treatment, which meets the EPA standard for arsenic in drinking water. Zn(1.0cur)O removed As(III) almost completely ($[As]_{180\ min}$ = 0.933 ppb) with the highest adsorption percent (98%) followed by Zn(2.0cur)O (96%) and Zn(0.5cur)O (92%). Bare ZnO removed ~52% of the initial arsenic concentration after half an hour ($[As]_{60\ min}$ ~ 20 ppb) and ~72% after 3 hours ($[As]_{180\ min}$ ~ 14.6 ppb) failing to take arsenic down its MCL. When the initial As(III) concentration was 903 ppb ~71 and 67% of As(III) could be removed with Zn(1.0cur)O and Zn(2.0cur)O respectively in 30 min (see Fig. 9b).

Even for such a high As(III) concentration, curcumin doped ZnO nanostructures demonstrated an excellent removal effect given the low loading of 42 ppb (0.04 g L^{-1}). As(III) equilibrium concentrations of about 180 ppb were left after the treatment period of 3 hours achieving almost similar ~75% removal for both curcumin contents. Therefore, highly efficient As(III) removal is possible with these curcumin doped ZnO sub-micro-granules requiring no pre-treatment (oxidation and/or pH adjustment) and post treatment pH adjustment. It is expected that doubling or tripling the loading amount will remove the 903 ppb arsenic contamination completely; even then the material loading is still considered economical.

To investigate the mechanism of As adsorption, the Lagergren pseudo first-order and Lagergren pseudo second-order equations were used to test the experimental data of different curcumin content in the Zn(cur)O adsorbent. The linearized pseudo-first-order equation can be presented as:[60]

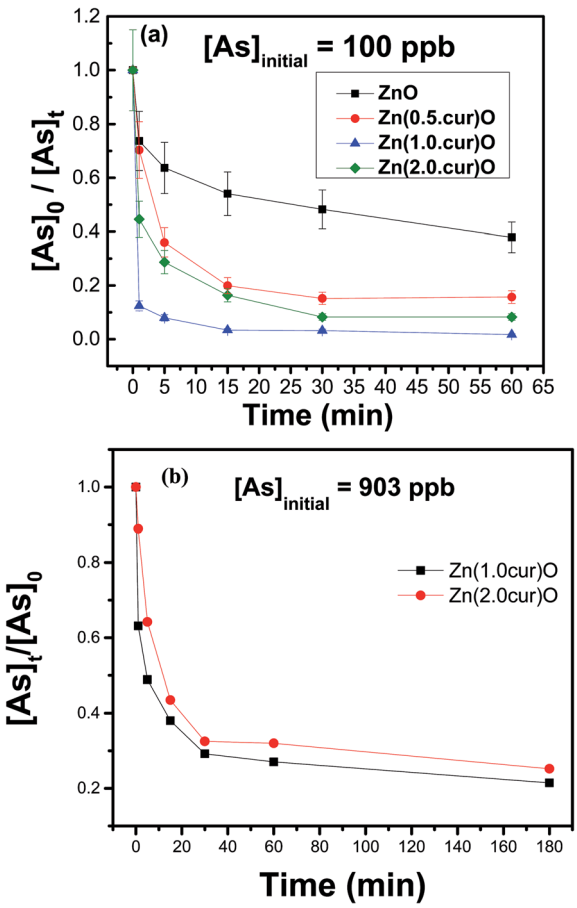

Fig. 9 Adsorption kinetics of As(III) on Zn(xcur)O and ZnO: (a) initial As(III) concentration was 100 μg L^{-1} and (b) initial As(III) concentration was 903 μg L^{-1}, the error margin was within 10%.

$$\ln(q_e - q_t) = -k_1 t + \ln q_e \quad (1)$$

where q_e and q_t are the capacities (mg g^{-1}) of arsenic adsorbed at equilibrium and at time t, respectively, and k_1 is the pseudo-first-order rate adsorption constant (mg g^{-1} min^{-1}). Plot of $\ln(q_e - q_t)$ *versus* t for an adsorbent yielded a straight line, usually governing the first 20–30 minutes of interaction, but the correlation coefficients (R) was poorer as shown in Fig. 10a and b. The rate constant was found to be dependent on the initial concentration of the adsorbate and varying greatly depending on the adsorption system.

The linearized pseudo-second-order equation is given as:

$$t/q_t = t/q_e + 1/(k_2 q_e^2) \quad (2)$$

k_2 is the pseudo-second-order rate constant and it depends on the operating conditions, such as initial pH and solution concentration, temperature, agitation rate, *etc.*[60] (all these parameters were kept constant for all the experiments). k_2 would decrease as the initial solution concentration increase as it takes a longer time to reach equilibrium. If the adsorption system follows a pseudo-second-order kinetics, then a plot of t/q_t *versus* t would be linear and k_2 and q_e can be determined from the intercept and slope of the graph eqn (2). In our case, the kinetic study results could be best fitted into a pseudo second-order rate kinetic model as demonstrated in Fig. 10c and d. The kinetic parameters obtained in fitting the experimental data are summarized in Tables 1 and 2. The applicability of the pseudo-second-order rate model was evaluated by the square of the correlation coefficient R (R^2), and its closeness to 1 indicates that the model fits the experimental data accurately. The correlation coefficients for the second-order kinetic model were greater than 0.999 for all the fits, which is better than first-order kinetic model (Fig. 10a and b). The sorption capacity of adsorbent was calculated by:

$$q_e = V(C_o - C_e)/m \quad (3)$$

where C_o and C_e are the initial and equilibrium concentration (mg L^{-1}) respectively, m is the mass of dry carbon sample used (g) and V volume of solution (mL). The calculated q_e values also agree very well with the experimental q_e.

Due to the differences in the experimental conditions, it is not possible to directly compare the adsorption efficiency among reports in literature. However, a rough comparison can be made. For instance, concerning relatively high arsenic concentrations, Yang and co-workers[59] synthesized ZnO microtubes, which have a large specific surface area. In their study,

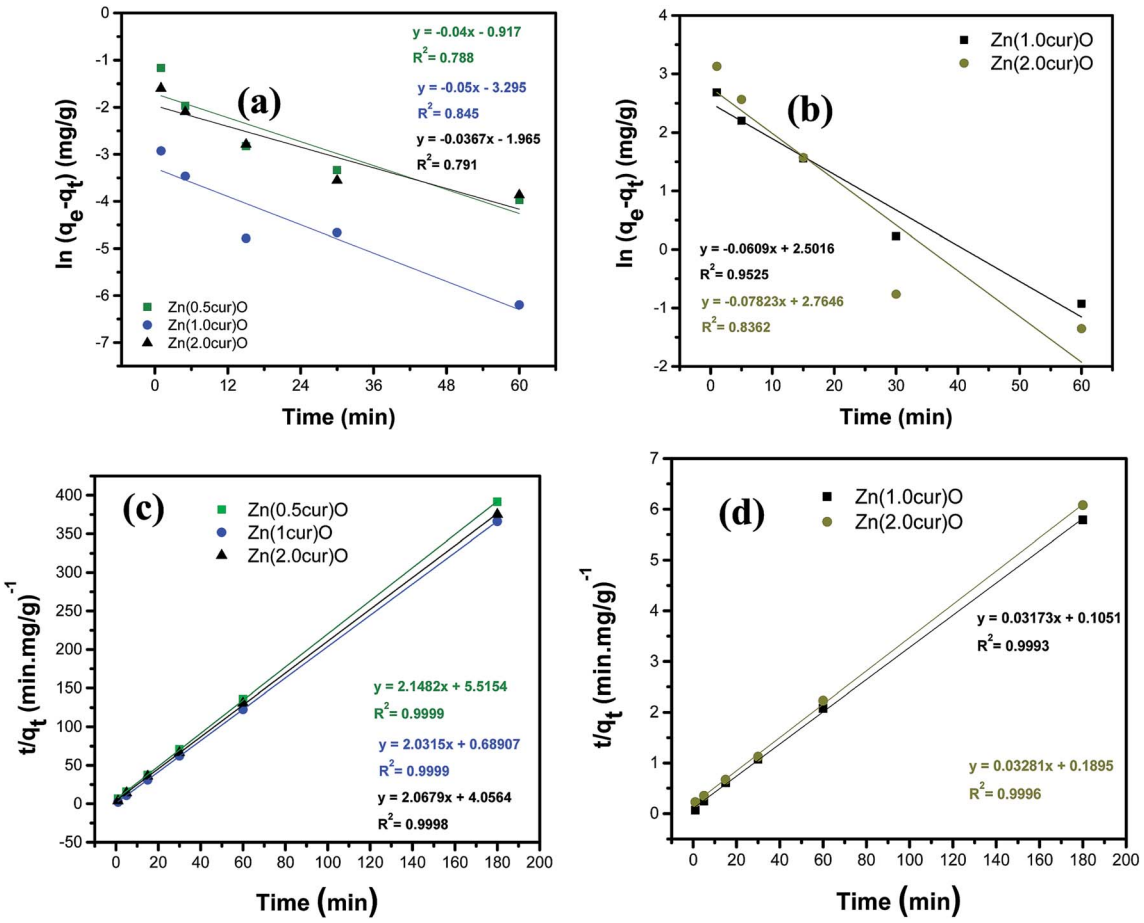

Fig. 10 (a) and (b) are pseudo-first-order rate kinetic model fitting of the adsorption kinetics studies demonstrated in Fig. 9a and b, respectively. (c) and (d) are pseudo-second-order rate kinetic model fitting of the adsorption kinetics studies demonstrated in Fig. 9a and b, respectively.

Table 1 Kinetic parameters of Zn(*x*cur)O nanostructures adsorption on As(III) at initial concentrations of 100 ppb

	$q_{e(cal)}$ (mg g^{-1})	$q_{e(exp)}$ (mg g^{-1})	K_{ad} (mg^{-1} g min^{-1})	R^2
Zn(0.5cur)O	0.4655	0.45972	0.8367	0.9999
Zn(1.0cur)O	0.4922	0.49146	5.9892	0.9999
Zn(2.0cur)O	0.4836	0.479645	1.0542	0.9996

Table 2 Kinetic parameters of Zn(*x*cur)O nanostructures adsorption on As(III) at initial concentrations of 903 ppb

	$q_{e(cal)}$ (mg g^{-1})	$q_{e(exp)}$ (mg g^{-1})	K_{ad} (mg g^{-1} min^{-1})	R^2
Zn(1.0cur)O	31.5160	29.2821	0.009579	0.9993
Zn(2.0cur)O	30.4785	27.177	0.005681	0.9996

the initial As(III) solution concentration was 0.9032 mg L^{-1}, pH value at 7.0, and the amount of ZnO loading at 0.08 g L^{-1}, the K_{ad} was determined at 0.005 mg^{-1} g min^{-1}; it increased to 0.015 mg^{-1} g min^{-1} upon loading with 0.1 g L^{-1}. In our study, having the same initial As(III) concentration, pH value at 6, and much lower adsorbent loading of 43 μg L^{-1}, the K_{ad} was determined to be higher (0.0096 and 0.0057 mg^{-1} g min^{-1} for Zn(1.0cur)O and Zn(2.0cur)O respectively) (see Table 2). For the low arsenic concentration range, the aforementioned study obtained 0.007 mg^{-1} g min^{-1} K_{ad} with an initial As(III) solution concentration of 0.0978 mg L^{-1}, pH value at 7.0, and the amount of ZnO loading at 0.01 g L^{-1} (10 mg L^{-1}). In comparison, for almost similar arsenic concentration of 0.1 mg L^{-1} and material loading 230 times less, we obtained much higher K_{ad} of 0.837, 5.99, and 1.05 mg^{-1} g min^{-1} (see Table 1) for curcumin contents of 0.5 mg, 1.0 mg, and 2.0 mg respectively. These ZnO micro-tubes themselves have surpassed the nanocrystalline TiO_2 with a large specific surface area of 330 m^2 g^{-1} synthesized by Meng and co-workers.[61,62] In their study, the initial As(III) solution concentration was 2.0 mg L^{-1}, the pH value was 7.0, and the amount of TiO_2 was 0.2 g L^{-1}. They reported K_{ad} to be 0.00025 mg^{-1} g min^{-1}. The surface area of the adsorbent is not the only property that ensures the efficiency of the adsorbent; other factors are critical which include the type and number of surface functional groups on the adsorbents. And as the surface area of these nanostructures is no greater than the nanocrystalline TiO_2 and probably the ZnO microtubes, these significant results suggest that curcumin conjugated ZnO nanostructures possess an excellent affiliation to As(III) due to the functionalities of the curcumin.

Since the rate for the reaction obeys pseudo second order kinetic model, the sorption capacity is proportional to the number of active sites occupied on the sorbent. Unlike the pseudo first order equation, the pseudo second order rate equation is likely to predict the behavior over the whole range of adsorption and the rate-limiting step is assumed to be chemical adsorption[63] involving valency forces through sharing or the exchange of electrons between the adsorbent and the metal ion. Therefore, the pseudo second order kinetics in present case suggests that the rate-limiting step is the surface adsorption, where the removal of As(III) from the solution is due to physicochemical interactions between the two phases. In our case the arsenic species present at pH 6 is H_3AsO_3. The As(III) species is thought to adsorb on the phenyl rings of curcumin and/or to the hydroxyls groups. Thus, we propose the possible reaction mechanisms as follows:

$$\text{Zn(cur–OH)O} + \text{As(III)} + \text{H}_2\text{O} \rightarrow 2\text{Zn(cur–OAs)O} + \text{H}_3\text{O}^+$$

or,

$$\text{Zn(cur–Ph)O} + \text{As(III)} \rightarrow \text{Zn(cur–Ph–As)O}$$

where Zn(cur–Ph)O and Zn(cur–OH)O is phenyl rings and hydroxyl group on the Zn(cur)O surface, respectively. One might argue that if this is the possible mechanism, then higher curcumin content should reflect a higher adsorption capacity, which is not seen in the results. In fact, the higher curcumin content (2 mg) incorporated in ZnO could be blocking the adsorption sites by stacking of phenyl rings or hydrogen bonding of hydroxyl groups of curcumin preventing adsorption of As(III). It is also important to note that dissolution of ZnO in water is about 1.6 to 7 mg L^{-1} depending on its size,[64,65] therefore, a small amount of zinc ion is expected to get release during treatment of wastewater. Though incorporation of curcumin is anticipated to reduce the dissolution of ZnO due to chelation between zinc ion and curcumin, further study needs to be done for practical use of such materials in wastewater treatment or environmental monitoring because small amount of zinc ion could be toxic to a variety of aquatic organisms.

4. Conclusions

Curcumin–ZnO hybrid materials were synthesized successfully using a wet chemistry procedure. The nanostructures were found to have sub-micro grain-like morphology and wurtzite hexagonal crystal structure of ZnO. They showed very good crystalline quality. FTIR spectra showed that curcumin chelates with zinc through enol form but at the same time a weak link between hydroxyl or methoxy groups on the phenyl ring and ZnO is not ruled out. The doping of curcumin into ZnO resulted in the enhancement of the exciton emission at 358 nm and the substantial decrease of the visible emission around 560 in comparison to ZnO photoluminescence. Curcumin seemed to fill defects that were visible luminescence centers and at the same time prolonged e–h recombination. In contrast to naked ZnO, Zn(cur)O could work as a fluorescence probe for arsenic sensing in the concentration ranges from 1 to 3000 ppb in water, however, the fluorescence response started saturating after 3000 ppb of arsenic in water. With a very low material loading, the Zn(cur)O nanostructures removed the As(III) contamination below the MCL from 100 ppb samples within 30 minutes, and almost to zero within 3 hours. Bare ZnO didn't bring down the arsenic contamination below its MCL even after

3 hours. The compound reached up to 75% removal/adsorption capacity with 903 ppb concentrations after 3 hours with the same loading, which reflects the excellent capacity of removal for such a high arsenic concentration by Zn(cur)O. Kinetics of adsorption fitted very well to pseudo second order model with exceptional adsorption rates that reflected the high affinity of the compound to As(III). Although Zn(cur)O could sense arsenic in the 0–3000 ppb concentration range by the fluorescence method rendering it a possible optical sensing materials and simultaneously offered an attractive alternative for a simple single-step treatment option to treat arsenic-contaminated natural water with high adsorption rates without the pre-treatment requirement for current industrial and environmental practices, controlling the size and shape of such Zn(cur)O nanomaterials would further improve such capabilities and applications.

Acknowledgements

Financial support provided by Lebanese National Council of Scientific Research (NCSR) and American University of Beirut, Lebanon through URB, Kamal A. Shair Research Fund as well as Kamal A. Shair Central Research Science Laboratory (KAS CRSL) facilities to carry out this work is greatly acknowledged.

References

1 R. Shenhar and V. M. Rotello, Nanoparticles: Scaffolds and Building Blocks, *Acc. Chem. Res.*, 2003, **36**(7), 549–561.
2 B. I. Ipe, K. Yoosaf and K. G. Thomas, Functionalized gold nanoparticles as phosphorescent nanomaterials and sensors, *J. Am. Chem. Soc.*, 2006, **128**(6), 1907–1913.
3 A. B. Djurišić and Y. H. Leung, Optical properties of ZnO nanostructures, *Small*, 2006, **2**(8–9), 944–961.
4 R. Janisch, P. Gopal and N. A. Spaldin, Transition metal-doped TiO_2 and ZnO—present status of the field, *J. Phys.: Condens. Matter*, 2005, **17**(27), R657.
5 R. Wahab, S. G. Ansari, Y. S. Kim, H. K. Seo, G. S. Kim, G. Khang and H. S. Shin, Low temperature solution synthesis and characterization of ZnO nano-flowers, *Mater. Res. Bull.*, 2007, **42**, 1640–1648.
6 J. Nishio, M. Tokumura, H. T. Znad and Y. Kawase, Photocatalytic decolorization of azo-dye with zinc oxide powder in an external UV light irradiation slurry photoreactor, *J. Hazard. Mater.*, 2006, **138**(1), 106–115.
7 Y. Li, G. W. Meng, L. D. Zhang and F. Philip, Ordered semiconductor ZnO nanowire arrays and their photoluminescence properties, *Appl. Phys. Lett.*, 2000, **76**, 2011–2017.
8 K. Omichi, K. Kaiya, N. Takahashi, T. Nakamura, S. Okamoto and H. Yamamoto, Growth of ZnO thin films exhibiting room-temperature ultraviolet emission by means of atmospheric pressure vapor-phase epitaxy, *J. Mater. Chem.*, 2001, **11**(2), 262–263.
9 A. H. Smith, E. O. Lingas and M. Rahman, Contamination of drinking-water by arsenic in Bangladesh: a public health emergency, *Bull. W. H. O.*, 2000, **78**, 1093–1103.
10 P. Kurttio, E. Pukkala, H. Kahelin, A. Auvinen and J. Pekkanen, Arsenic concentrations in well water and risk of bladder and kidney cancer in Finland, *Environ. Health Perspect.*, 1999, **107**(9), 705.
11 Y. Xia and J. Liu, An overview on chronic arsenism *via* drinking water in PR China, *Toxicology*, 2004, **198**(1), 25–29.
12 K. Saha, Review of arsenicosis in west Bengal, India—a clinical perspective, *Crit. Rev. Environ. Sci. Technol.*, 2003, **33**(2), 127–163.
13 A. H. Welch, M. S. Lico and J. L. Hughes, Arsenic in ground water of the western United States, *Groundwater*, 1988, **26**(3), 333–347.
14 N. E. Korte and Q. Fernando, A review of arsenic(III) in groundwater, *Crit. Rev. Environ. Control*, 1991, **21**, 1–11.
15 T. S. Choong, T. Chuah, Y. Robiah, F. Gregory Koay and I. Azni, Arsenic toxicity, health hazards and removal techniques from water: an overview, *Desalination*, 2007, **217**(1), 139–166.
16 S. Goldberg, Competitive adsorption of arsenate and arsenite on oxides and clay minerals, *Soil Sci. Soc. Am. J.*, 2002, **66**(2), 413–421.
17 B. Saha, R. Bains and F. Greenwood, Physicochemical characterization of granular ferric hydroxide (GFH) for arsenic(V) sorption from water, *Sep. Sci. Technol.*, 2005, **40**(14), 2909–2932.
18 M. Borho and P. Wilderer, Optimized removal of arsenate(III) by adaptation of oxidation and precipitation processes to the filtration step, *Water Sci. Technol.*, 1996, **34**(9), 25–31.
19 H. Lee and W. Choi, Photocatalytic oxidation of arsenite in TiO_2 suspension: kinetics and mechanisms, *Environ. Sci. Technol.*, 2002, **36**(17), 3872–3878.
20 Y. Kim, C. Kim, I. Choi, S. Rengaraj and J. Yi, Arsenic removal using mesoporous alumina prepared *via* a templating method, *Environ. Sci. Technol.*, 2004, **38**(3), 924–931.
21 L. S. McNeill and M. Edwards, Review of iron pipe corrosion in drinking water distribution systems, *J. Am. Water Works Assoc.*, 2001, **93**(7), 88–100.
22 J. G. Hering, P.-Y. Chen, J. A. Wilkie, M. Elimelech and S. Liang, Arsenic removal by ferric chloride, *J. Am. Water Works Assoc.*, 1996, **88**(4), 155–167.
23 S. P. Pande, L. S. Deshpande, P. Patni and S. Lutade, Arsenic removal studies in some ground waters of West Bengal, India, *J. Environ. Sci. Health, Part A: Environ. Sci. Eng. Toxic Hazard. Subst. Control*, 1997, **32**(7), 1981–1987.
24 R. Qiu, D. Zhang, Y. Mo, L. Song, E. Brewer, X. Huang and Y. Xiong, Photocatalytic activity of polymer-modified ZnO under visible light irradiation, *J. Hazard. Mater.*, 2008, **156**(1), 80–85.
25 S. H. Liao, H. J. Jhuo, Y. S. Cheng and S. A. Chen, Fullerene Derivative-Doped Zinc Oxide Nanofilm as the Cathode of Inverted Polymer Solar Cells with Low-Bandgap Polymer (PTB7-Th) for High Performance, *Adv. Mater.*, 2013, **25**(34), 4766–4771.
26 Z. Li, Y. Xiong and Y. Xie, Selected-control synthesis of ZnO nanowires and nanorods *via* a PEG-assisted route, *Inorg. Chem.*, 2003, **42**(24), 8105–8109.

27 R. Hariharan, S. Senthilkumar, A. Suganthi and M. Rajarajan, Photodynamic action of curcumin derived polymer modified ZnO nanocomposites, *Mater. Res. Bull.*, 2012, **47**, 3090–3099.

28 R. Könenkamp, R. C. Word and C. Schlegel, Vertical nanowire light-emitting diode, *Appl. Phys. Lett.*, 2004, **85**(24), 6004–6006.

29 A. Goel, A. B. Kunnumakkara and B. B. Aggarwal, Curcumin as "Curecumin": From kitchen to clinic, *Biochem. Pharmacol.*, 2008, **75**(4), 787–809.

30 B. B. Aggarwal and K. B. Harikumar, Potential therapeutic effects of curcumin, the anti-inflammatory agent, against neurodegenerative, cardiovascular, pulmonary, metabolic, autoimmune and neoplastic diseases, *Int. J. Biochem. Cell Biol.*, 2009, **41**(1), 40–59.

31 R. M. Srivastava, S. Singh, S. K. Dubey, K. Misra and A. Khar, Immunomodulatory and therapeutic activity of curcumin, *Int. Immunopharmacol.*, 2011, **11**(3), 331–341.

32 T. Ganesh, J. H. Kim, S. J. Yoon, B.-H. Kil, N. N. Maldar, J. W. Han and S.-H. Han, Photoactive curcumin-derived dyes with surface anchoring moieties used in ZnO nanoparticle-based dye-sensitized solar cells, *Mater. Chem. Phys.*, 2010, **123**(1), 62–66.

33 D. Patra and C. Barakat, Unique role of ionic liquid [bmin] [BF_4] during curcumin–surfactant association and micellization of cationic, anionic and non-ionic surfactant solutions, *Spectrochim. Acta, Part A*, 2011, **79**, 1823–1828.

34 M. Mouslmani, K. H. Bouhadir and D. Patra, Poly(9-(2-diallylaminoethyl)adenine HCl-*co*-sulfur dioxide) deposited on silica nanoparticles constructs hierarchically ordered nanocapsules: curcumin conjugated nanocapsules as a novel strategy to amplify guanine selectivity among nucleobases, *Biosens. Bioelectron.*, 2015, **68**, 181–188.

35 D. Patra, R. Aridi and K. Bouhadir, Fluorometric sensing of DNA using curcumin encapsulated nanoparticles assembled microcapsules from poly(diallyl ammonium chloride-*co*-sulfur dioxide), *Microchim. Acta*, 2013, **180**, 59–64.

36 D. Patra, E. El Khoury, D. Ahmadieh, S. Darwish and R. M. Tafech, Effect of Curcumin on Liposome: Curcumin as a Molecular Probe for Monitoring Interaction of Ionic Liquids with 1,2-Dipalmitoyl-*sn-glycero*-3-phosphocholine Liposome, *Photochem. Photobiol.*, 2012, **88**, 317–327.

37 E. El Khoury, M. Abiad, Z. G. Kassaify and D. Patra, Green synthesis of curcumin conjugated nanosilver for the applications in nucleic acid sensing and anti-bacterial activity, *Colloids Surf., B*, 2015, **117**, 274–280.

38 R. N. Moussawi and D. Patra, Synthesis of Au Nanorods through Pre-Reduction with Curcumin: Preferential Enhancement of Au Nanorods Formation Prepared from CTAB Capped over Citrate Capped Au Seeds, *J. Phys. Chem. C*, 2015, **119**, 19458–19468.

39 S.-S. Zhou, X. Xue, J.-F. Wang, Y. Dong, B. Jiang, D. Wei, M.-L. Wan and Y. Jia, Synthesis, optical properties and biological imaging of the rare earth complexes with curcumin and pyridine, *J. Mater. Chem.*, 2012, **22**, 22774–22780.

40 A. Ciszewski, G. Milczarek, B. Lewandowska and K. Krutowski, Electrocatalytic properties of electropolymerized Ni(II) curcumin complex, *Electroanalysis*, 2003, **15**, 518–523.

41 A. K. Renfrew, N. S. Bryce and T. W. Hambley, Delivery and release of curcumin by a hypoxia-activated cobalt chaperone: a XANES and FLIM study, *Chem. Sci.*, 2013, **4**, 3731–3739.

42 M. I. Khalil, A. M. Al-Zahem and M. M. Qunaibit, Synthesis, characterisation and antitumor activity of binuclear curcumin–metal(II) hydroxo complexes, *Med. Chem. Res.*, 2014, **23**, 1683–1689.

43 M. I. Khalil, M. M. Al-Qunaibit, A. M. Al-zahem and J. P. Labis, Synthesis and characterization of ZnO nanoparticles by thermal decomposition of a curcumin zinc complex, *Arabian J. Chem.*, 2014, **7**, 1178–1184.

44 R. Dhivya, J. Ranjani, J. Rajendhran, M. Rajasekaran and J. Annaraj, pH responsive curcumin/ZnO nanocomposites for drug delivery, *Adv. Mater. Lett*, 2015, **6**, 505–512.

45 L. Upadhyaya, J. Singh, V. Agarwal, A. C. Pandey, S. P. Verma, P. Das and R. P. Tewari, Efficient water soluble nanostructured ZnO grafted chitosan/curcumin-nanocomposites for cancer therapy, *Process Biochem.*, 2015, **50**, 678–688.

46 E. El Khoury and D. Patra, Ionic liquid expedites partition of curcumin into solid gel but discourages into liquid crystalline phases of 1,2-dimyristoyl-*sn-glycero*-3-phosphocholine liposome, *J. Phys. Chem. B*, 2013, **117**, 9699–9708.

47 K. Mishra, R. K. Srivastava and S. G. Prakash, Photoluminescence and photoconductivity studies of ZnO nanoparticles prepared by solid state reaction method, *J. Mater. Sci.: Mater. Electron.*, 2013, **24**, 125–134.

48 S. N. A. El-Rahman and S. S. Al-Jameel, Protection of Curcumin and Curcumin Nanoparticles against Cisplatin Induced Nephrotoxicity in Male Rats, *Scholars Academic Journal of Biosciences*, 2014, **2**(3), 214–223.

49 Z. Lu, J. Zhou, A. Wang, N. Wang and X. Yang, Synthesis of aluminium-doped ZnO nanocrystals with controllable morphology and enhanced electrical conductivity, *J. Mater. Chem.*, 2011, **21**(12), 4161–4167.

50 H.-M. Xiong, R.-Z. Ma, S.-F. Wang and Y.-Y. Xia, Photoluminescent ZnO nanoparticles synthesized at the interface between air and triethylene glycol, *J. Mater. Chem.*, 2011, **21**(9), 3178–3182.

51 T. M. Kolev, E. A. Velcheva, B. A. Stamboliyska and M. Spiteller, DFT and experimental studies of the structure and vibrational spectra of curcumin, *Int. J. Quantum Chem.*, 2005, **102**(6), 1069–1079.

52 S. Buddee, S. Wongnawa, P. Sriprang and C. Sriwong, Curcumin-sensitized TiO_2 for enhanced photodegradation of dyes under visible light, *J. Nanopart. Res.*, 2014, **16**(4), 1–21.

53 S. Tayyari, H. Rahemi, A. Nekoei, M. Zahedi-Tabrizi and Y. Wang, Vibrational assignment and structure of dibenzoylmethane: a density functional theoretical study, *Spectrochim. Acta, Part A*, 2007, **66**(2), 394–404.

54 K. Krishnankutty and V. D. John, Synthesis, characterization and antitumor studies of metal chelates of some synthetic curcuminoids, *Synth. React. Inorg. Met.-Org. Chem.*, 2003, **33**, 343–358.

55 H.-M. Xiong, Photoluminescent ZnO nanoparticles modified by polymers, *J. Mater. Chem.*, 2010, **20**(21), 4251–4262.

56 J. Zhang, H. Liu, Z. Wang, N. Ming, Z. Li and A. S. Biris, Polyvinylpyrrolidone-Directed Crystallization of ZnO with Tunable Morphology and Bandgap, *Adv. Funct. Mater.*, 2007, **17**(18), 3897–3905.

57 S. H. Mousavi, H. Haratizadeh and H. Minaee, The effect of morphology and doping on photoluminescence of ZnO nanostructures, *Opt. Commun.*, 2011, **284**(14), 3558–3561.

58 S. Srivastava and Y. Srivastav, Removal of Arsenic from Waste Water by Using ZnO Nano-Materials, *J. Mater. Sci. Eng. B*, 2003, **3**(8), 483–492.

59 W. Yang, Q. Li, S. Gao and J. K. Shang, High efficient As(III) removal by self-assembled zinc oxide micro-tubes synthesized by a simple precipitation process, *J. Mater. Sci.*, 2011, **46**(17), 5851–5858.

60 M.-S. Chiou and H.-Y. Li, Equilibrium and kinetic modeling of adsorption of reactive dye on cross-linked chitosan beads, *J. Hazard. Mater.*, 2002, **93**(2), 233–248.

61 S. Bang, M. Patel, L. Lippincott and X. Meng, Removal of arsenic from ground water by granular titanium dioxide adsorbent, *Chemosphere*, 2005, **60**, 389–397.

62 G. Huan, J. du, X. Meng, Y. Sun, B. Sun and Q. Hu, Application of titanium dioxide in arsenic removal from water: a review, *J. Hazard. Mater.*, 2012, **215–216**, 1–16.

63 Y.-S. Ho and G. McKay, Pseudo-second order model for sorption processes, *Process Biochem.*, 1999, **34**(5), 451–465.

64 S. W. Wong, P. T. Leung, A. B. Djursić and K. M. Leung, Toxicities of nano zinc oxide to five marine organism: influence of aggregates size and ion solubility, *Anal. Bioanal. Chem.*, 2010, **396**, 609–618.

65 R. B. Seed, D. A. Ladner, C. P. Higgins, P. Wsterhoff and J. F. Ranville, Solubility of nano-zinc oxide in environmentally and biologically important matrices, *Environ. Toxicol. Chem.*, 2012, **31**, 93–99.